

NUMERICAL SIMULATIONS OF WIND ACCRETION IN SYMBIOTIC BINARIES

M. DE VAL-BORRO¹, M. KAROVSKA AND D. SASSELOV

Harvard-Smithsonian Center for Astrophysics, 60 Garden St., Cambridge, MA 02138, USA

Draft version November 4, 2018

ABSTRACT

About half of the binary systems are close enough to each other for mass to be exchanged between them at some point in their evolution, yet the accretion mechanism in wind accreting binaries is not well understood. We study the dynamical effects of gravitational focusing by a binary companion on winds from late-type stars. In particular, we investigate the mass transfer and formation of accretion disks around the secondary in detached systems consisting of an AGB mass-losing star and an accreting companion. The presence of mass outflows is studied as a function of mass loss rate, wind temperature and binary orbital parameters. A 2-dimensional hydrodynamical model is used to study the stability of mass transfer in wind accreting symbiotic binary systems. In our simulations we use an adiabatic equation of state and a modified version of the isothermal approximation, where the temperature depends on the distance from the mass losing star and its companion. The code uses a block-structured adaptive mesh refinement method that allows us to have high resolution at the position of the secondary and resolve the formation of bow shocks and accretion disks. We explore the accretion flow between the components and formation of accretion disks for a range of orbital separations and wind parameters. Our results show the formation of stream flow between the stars and accretion disks of various sizes for certain orbital configurations. For a typical slow and massive wind from an AGB star the flow pattern is similar to a Roche lobe overflow with accretion rates of 10% of the mass loss from the primary. Stable disks with exponentially decreasing density profiles and masses of the order 10^{-4} solar masses are formed when wind acceleration occurs at several stellar radii. The disks are geometrically thin with eccentric streamlines and close to Keplerian velocity profiles. The formation of tidal streams and accretion disks is found to be weakly dependent on the mass loss from the AGB star. Our simulations of gravitationally focused wind accretion in symbiotic binaries show the formation of stream flows and enhanced accretion rates onto the compact component. We conclude that mass transfer through a focused wind is an important mechanism in wind accreting interacting binaries and can have significant impact on the evolution of the binary itself and the individual components.

Subject headings: Accretion, accretion disks – Binaries: symbiotic – Hydrodynamics – Methods: numerical – Stars: mass loss – Stars: winds, outflows

1. INTRODUCTION

Accretion is a very important energy source for a wide variety of astronomical objects including many interacting binaries. The mass transfer in interacting binaries usually occurs via tidal interaction and Roche lobe overflow (RLOF). However, a wide range of interacting binaries belong to a class of accreting systems where the primary does not fill its Roche surface, and the mass transfer is believed to occur mostly by wind accretion. These include many symbiotic binaries and even more exotic systems such as massive X-ray binaries and microquasars. Wind accretion is more complicated than tidal interaction, and the accretion processes in wind accreting binaries are poorly understood. In this paper, we study gravitationally focused wind accretion in symbiotic systems with an AGB star and a compact accretor where the photosphere of the primary does not fill its Roche lobe.

Symbiotic binaries are important astrophysical laboratories for studies of wind accretion because of the wide separation of the components, and the ability to study the individual components and the accretion processes at many wavelengths ranging from X-ray to radio (Karovska et al. 1997, 2005; Matthews & Karovska 2006). A typical symbiotic consists of a mass-losing AGB or a red giant star and a hot accreting companion, often a white dwarf (WD). The components in these systems are assumed to be detached (at least during most of the orbital motion) and the compact companion accretes mass from the massive wind of the cool evolved star.

Mass loss is known to be a key factor in the late stages of the evolution of an AGB star. Matter escapes easily because of the low surface gravity. As the intermediate mass stars enter the AGB phase their atmospheres rise to sizes of the order of few AU. These stars become unstable to large amplitude radial pulsations and drive strong shock waves that produce an extended envelope and a copious stellar wind driven by radiation pressure on dust grains that form at several stellar radii above the photosphere (Bowen 1988). The powerful stellar winds also affect the evolution of the ISM by influencing its dynamics and spreading elements generated in stellar interiors. It is believed that interstellar dust has its origin in cool atmospheres and dense winds blowing from these evolved stars.

Due to massive stellar winds, intermediate mass stars can avoid exploding as a supernova and become planetary nebulae (PN) and proto-planetary nebulae (PPN) at the end of the AGB (see e.g. Gawryszczak et al. 2002). Mass-losing giant stars and PPNs often present asymmetric envelopes and bipolar outflows that can be explained by wind gravitational focusing and wind collision dynamics. The presence of bipolar and collimated outflows in PPNs has been explained due to a collision of stellar winds (Mellema & Frank 1997; González et al. 2004) and magnetically driven jets (Blackman et al. 2001).

In the following we show that although the photosphere of the AGB star in symbiotic systems does not fill its Roche lobe, its extended atmosphere can be significantly disturbed by the accreting companion. Mass accretion can be increased due to the gravitational attraction from the accretor and the centrifugal force due to the rotation of the system. This is important, because the binary parameters can evolve which will affect

¹ Stockholm University, AlbaNova University Center, SE-106 91, Stockholm, Sweden

the stellar mass loss and wind parameters. Mass and angular momentum can be lost from the system or accreted onto the companion. The angular momentum loss can result in orbital shrinking of the system which would enhance mass transfer and can lead to a Type Ia supernova (Hachisu et al. 1999; Jahanara et al. 2005; Podsiadlowski & Mohamed 2007). The evolution of AGB stars in binary systems gives rise to highly aspherical winds and can be significantly different from that of single stars.

We use 2-dimensional hydrodynamical time-dependent models to investigate the mass transfer driven by a massive AGB wind that is captured by a detached companion star. We calculate accretion rates assuming wind acceleration at different radii of the extended atmosphere (dust formation radii) and also consider the case when the extended envelope reaches the Lagrangian point L_1 and the gas flows in a narrow stream towards the secondary. In Section 2, we discuss Bondy-Hoyle wind accretion in a symbiotic systems with an AGB mass-losing star. We describe our numerical setups in Section 3. In Section 4 we present the results of the numerical simulations and we compare the theoretical models with recent observations of symbiotic binaries to improve our understanding of the properties of these systems. Finally, we discuss the results and future work in Section 5.

2. BONDI-HOYLE ACCRETION

Physical processes involved in winds from extended atmospheres are very complex and only recently a detailed theoretical modeling has been possible (see e.g. Bowen & Willson 1991; Arndt et al. 1997; Mastrodemos & Morris 1998; Sandin & Höfner 2004; Freytag & Höfner 2008). In the classical theory of plane-parallel stellar atmospheres the physical structure of the atmosphere is determined by the effective temperature and surface gravity for a given chemical composition of the atmosphere. In the case of the AGB stars the situation becomes more complex. Pulsations in the atmosphere, phenomena generated in the stellar interior such as convection, and especially dust formation influence the mass loss and wind parameters.

For high velocity winds where the pressure can be neglected, the Bondi-Hoyle accretion rate is given by (see Edgar 2004, for a recent review of Bondi-Hoyle-Lyttleton accretion)

$$\dot{M}_{\text{BH}} = \pi R_a^2 \rho_B v_r, \quad (1)$$

where ρ_B is density at the secondary's position, $v_r = \sqrt{v_w^2 + v_B^2}$ is the wind velocity relative to the accreting object, v_w is the wind velocity at the position of the secondary, v_B is the orbital velocity of the companion, and R_a is the Bondi-Hoyle accretion radius given by

$$R_a = \frac{2GM_B}{v_r^2}. \quad (2)$$

When the mass accretion rate is normalized to the 2-dimensional case we obtain

$$\dot{M}_{\text{BH}} = 2R_a \rho_B v_r. \quad (3)$$

The mass loss from the unperturbed wind of the AGB component in the orbital plane at the secondary position is

$$\dot{M}_{\text{wind}} = 2\pi d \rho_B v_w. \quad (4)$$

Therefore the Bondi-Hoyle accretion ratio, defined as the mass accretion divided by the mass loss rate from the primary,

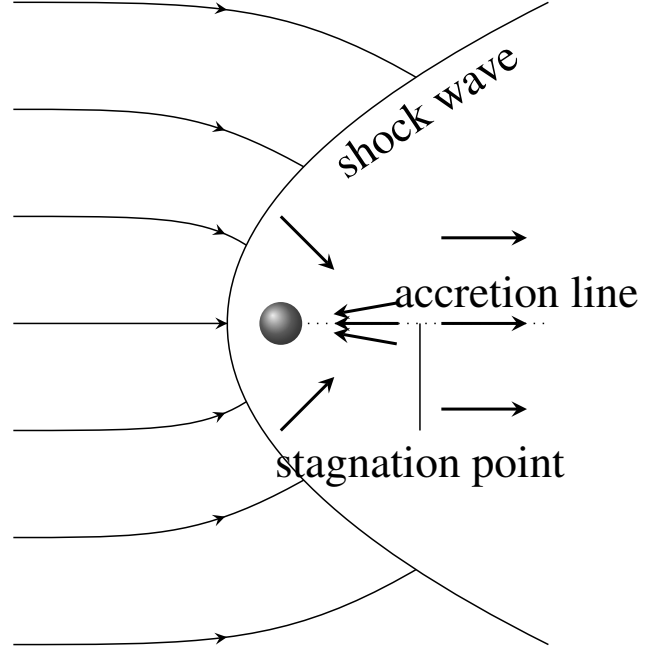


Fig. 1.— Diagram of the accretion geometry around the secondary marked by the gray circle. The flow is deflected at the shock wave and most of the accretion takes place along the accretion line behind the accretor.

in our 2-dimensional model is given by

$$f_{\text{BH}} = \frac{\dot{M}_{\text{BH}}}{\dot{M}_{\text{wind}}} = \frac{\Omega_b^2 d^2}{\pi v_r v_w (1+q)}, \quad (5)$$

with q denoting the mass ratio, d the binary separation and we have used the definition of the orbital Keplerian frequency

$$\Omega_b = \left(\frac{G(M_A + M_B)}{d^3} \right)^{1/2}. \quad (6)$$

As we will see in Section 4.2, the fraction of the AGB wind accreted by the secondary is several times higher than the Bondi-Hoyle rate in our simulations due to gravitational wind focusing. However, the Bondi-Hoyle theory cannot be directly applied to the wind accretion scenario in the case of slow winds where the sound speed is not negligible.

If the gas pressure is included in the Bondi-Hoyle scenario (Bondi 1952; Theuns & David 1992), the mass accretion ratio in the orbital plane becomes

$$f_{\text{BH}} = \frac{\Omega_b^2 d^2}{\pi v_r v_w (1+q)} \left(\frac{\mathcal{M}}{1+\mathcal{M}^2} \right)^{3/2}, \quad (7)$$

where \mathcal{M} is the Mach number

$$\mathcal{M} = \frac{v_w}{c_s}, \quad (8)$$

and c_s is the sound speed. The accretion radius is defined as

$$R_a = \frac{2GM_B}{v_r^2 + c_s^2}. \quad (9)$$

A diagram of the flow structure in the orbital plane is shown in Fig. 1. The stellar wind flows from the left and impacts the shock wave and is deflected towards the accreting companion. In the Bondi-Hoyle picture, the gas reaches the accretion line where the transversal velocity component is neglected and the

gravitationally bounded material is accreted. In our wind accretion model the AGB photosphere does not fill its Roche lobe and the mass loss is carried out in the form of a slow wind from the region where dust grains are condensed.

The wind in our models is characterized by a typical AGB mass-loss rate $\dot{M} \sim 10^{-9} - 10^{-6} M_{\odot} \text{ yr}^{-1}$ (Ryde et al. 2000) and the unperturbed initial velocity profile is given by the isothermal wind solution. In our slower wind models the Bondi accretion radius is comparable to the stellar separation and Bondi-Hoyle theory is not valid. Nevertheless, we will use the Bondi-Hoyle rates to compare with the mass accretion rates resulting from our simulations.

3. NUMERICAL MODEL

Two different problems in the context of mass loss in late stages of stellar evolution are investigated. In the first case the primary's extended envelope fills its Roche lobe and the gas flows in a narrow stream towards the secondary. This could be the case when the companion is in periastron. We also use this model to test our numerical model. Mass transfer in the second model is driven by a massive wind that is captured by a detached companion star. This is an important mechanism for the formation of accretion disks in detached interacting binaries, symbiotic stars and massive X-ray binaries (see e.g. Livio & Warner 1984; Soker 2004).

We follow the gas flow in the orbital plane of the system using 2-dimensional hydrodynamical simulations that allows us to resolve the large density contrasts close to the secondary. We limit our wind accreting model to the orbital plane of the binary system where the wind is focused forming an equatorial outflow that has a significant density enhancement compared with the regions further polewards (Walder et al. 2008). In Fig. 2, we show a diagram of the Roche potential in the equatorial plane for a mass ratio $q = 1$.

The basic equations of hydrodynamics describing the evolution of the density and velocity field are:

$$\frac{\partial \rho}{\partial t} + \nabla \cdot (\rho \mathbf{v}) = 0 \quad (10)$$

$$\frac{\partial \mathbf{v}}{\partial t} + (\mathbf{v} \cdot \nabla) \mathbf{v} = -\frac{1}{\rho} \nabla p - \nabla \Phi, \quad (11)$$

where ρ is the density in the orbital plane, \mathbf{v} the velocity of the fluid, p the pressure and Φ the gravitational potential. Both stellar gravity potentials were approximated as point masses. To avoid numerical problems close to the stars the potential is softened using the function:

$$\Phi = \Phi_A + \Phi_B = -\frac{GM_A}{\sqrt{|\mathbf{r} - \mathbf{r}_A|^2 + \epsilon^2}} - \frac{GM_B}{\sqrt{|\mathbf{r} - \mathbf{r}_B|^2 + \epsilon^2}}. \quad (12)$$

where the smoothing length ϵ was set to 0.01 length units in our simulations with standard resolution. The unit of length in our calculations corresponds to the separation between the stars. In our higher resolution simulations the number of grid zones in the accretion region was ~ 200 . The surface of the compact accretor was not resolved in our models.

3.1. Numerical code

Our code is based on FLASH (Fryxell et al. 2000), which is a fully parallel block-structured Adaptive Mesh Refinement (AMR) implementation of the Piecewise Parabolic Method (PPM) algorithm (Woodward & Colella 1984; Colella &

Woodward 1984) in its original Eulerian form². The code has been extensively tested in various compressible flow problems with astrophysical applications (see e.g. Calder et al. 2002; de Val-Borro et al. 2006).

For numerical convenience we introduce dimensionless units, where the binary separation d is taken as the unit of length. The unit of time is calculated from the orbital angular frequency Ω_b of the system. The orbital period of the system is then defined by

$$P_b = 2\pi. \quad (13)$$

Each simulation was run for about 10 orbital periods, when the system has reached a quasi-equilibrium state. The evolutionary time of the results discussed in Section 4 will be given in units of P_b .

We normalize all physical quantities for numerical convenience. The gravitational constant G is set to one as is done frequently in relativistic calculations. Eq. 6 can be considered as a normalization condition for the unit of mass to be the sum of the stellar masses $M = M_A + M_B$.

Our implementation of the FLASH code uses polar coordinates and was run in both the coordinate system corotating with the angular speed of the system and in the inertial frame. In addition to the usual hydrodynamic quantities, our model includes the gravity of both stars, and the Coriolis and centrifugal forces. The code is based on release 2.5 of FLASH with customized modules for the equation of state and gravity forces that explicitly conserve angular momentum transport (Kley 1998). This is particularly important when large density gradients are present in the wind. The Coriolis forces were treated conservatively as described by Kley (1998). A Courant number of 0.7 was used in the simulations. We use an equation of state for an ideal gas with ratio of specific heats between $\gamma = 1 - 5/3$ to represent more realistic cases that include radiative cooling, and a modified isothermal Riemann solver ported from the AMRA code (Plewa & Müller 2001).

We ignore magnetic fields, radiation transfer or explicit Navier-Stokes viscosity in our models. FLASH has a small numerical viscosity that has been estimated by de Val-Borro et al. (2007). Non-axisymmetric effects on the tidally enhanced wind may be caused by magnetic fields. It is likely that stellar winds in AGB stars are primarily radial since the extended envelope cannot have significant rotation (Soker & Zoabi 2002). The MHD collimation of the wind is a very efficient mechanism and can be more important than gravitational focusing (García-Segura & López 2000; García-Segura et al. 2001). However, MHD effects are not included in our calculations since there are presently no constraints on the magnetic fields in symbiotic systems. At the AGB phase, it is unlikely that a globally ordered magnetic field strongly affects the dynamics of the wind.

3.2. Mass accretion onto the secondary

The formation of an accretion disk can be affected by accretion onto the secondary. In the case of a reflecting boundary the stream bounces off the stellar surface and orbits the accretor. However, if no mass is allowed to accrete onto the secondary the orbiting disk continues to increase as the simulation continues. We use a mechanism that allows us to remove gas from the vicinity of the secondary. The accretion is accounted for by removing some mass from the region defined by $|\mathbf{r} - \mathbf{r}_B| < r_{\text{acc}}$ and adding it to the mass of the star

² The FLASH code is available at <http://www.flash.uchicago.edu/>

to calculate the gravitational forces. The goal was to obtain a quasi-stable configuration and to be able to estimate the accretion rate onto the accretor. The size of the accretion region r_{acc} is defined as a fraction of the Hill radius of the mass accretor. In most of our simulations the accretion radius is $r_{\text{acc}} = 0.1R_{\text{H}}$, where R_{H} is the Hill radius of the secondary

$$R_{\text{H}} = d \left(\frac{M_{\text{B}}}{3M_{\text{A}}} \right)^{1/3}. \quad (14)$$

The mass is removed from the disk after each time step using the expression (Günther & Kley 2002)

$$\Delta\rho = \min(0, f\Delta t) \max(0, \rho - \rho_{\text{av}}), \quad (15)$$

where f is a constant fraction of the order unity, Δt denotes the timestep and ρ_{av} is the average density in the region $r_{\text{acc}} < |\mathbf{r} - \mathbf{r}_{\text{B}}| < 2r_{\text{acc}}$ following Pepliński et al. (2008). The momentum of the accreted material is removed from the system.

We calculate the mass accretion ratio as the ratio of mass captured by the companion to the mass loss rate from the primary averaged over 100 timesteps

$$f = \left\langle \frac{\dot{M}_{\text{acc}}}{\dot{M}_{\text{wind}}} \right\rangle. \quad (16)$$

Theuns et al. (1996) have found accretion efficiencies around 2% for binaries with mass ratio $q = 2$.

3.3. Roche lobe overflow

Some of the most dramatic phenomena in binary systems occur when an AGB star fills its Roche lobe. In this case, a dynamically unstable mass transfer to the companion takes place that can lead to the formation of a common envelope and a very fast evolution of the binary system. We model the interaction of a tidal L_1 stream with an accretion disk around a compact star using an adiabatic equation of state and an isothermal solver to compare the results with the wind accretion simulations and test our numerical code.

The density of the stream flowing from the Lagrangian inner point has the form.

$$\rho = \rho_0 + \frac{\rho_s - \rho_0}{\cosh((\phi/\phi_0)^m)} \quad (17)$$

where ρ_0 is the initial unperturbed density, ρ_s is the density of the stream, ϕ_0 is the azimuthal angle of the inner Lagrangian point and m is a coefficient of order 20 that gives the steepness of the stream.

The initial radial velocity was of the order 1% of the orbital velocity of the system and directed towards the mass accreting companion. We have checked that different initial velocities at the L_1 point do not affect our results. According to the analytical calculations of Lubow & Shu (1975), the tidal stream leaves the first Lagrangian point at an incidence angle of approximately 28° with respect to the line joining the centers of the two stars. Since the unit of density ρ_0 drops out of the equations of motion, we may normalize it to any specified density. It is useful to set the stream density to a fraction of the total mass of the system to be able to compare accretion rates to the initial mass.

We used two different boundary conditions at the inner edge of the grid. The stream flow and formation of an accretion disk depend on the interaction of the tidal stream with the surface of the accreting star. Therefore it is important to test different boundary conditions at the surface of this star. We

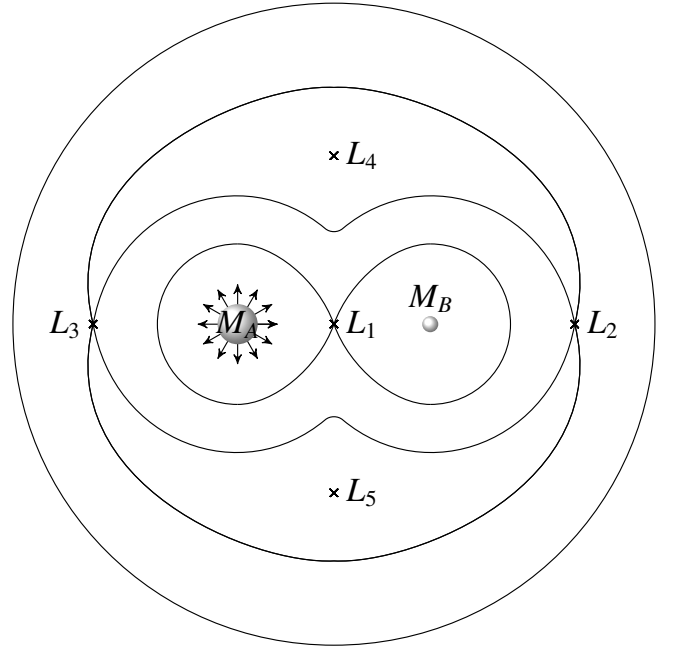


FIG. 2.— Roche potential on the orbital plane showing the location of the Lagrangian points for a mass ratio $q = 1$.

used reflecting boundary and allowed accretion onto the star using the prescription defined in Section 3.2 and an absorbing boundary where the radial gradients of the velocity pressure, and density are zero at the inner boundary. Simulations using an absorbing boundary allow the stream to flow into the accretor without generating reflected waves. We assume that the computational domain is filled with tenuous gas with the temperature profile of the wind. Initially, the density of the ambient material is 10 orders of magnitude smaller than the density at the surface of the mass-losing star.

The hydrodynamic flow was computed in cylindrical coordinates centered on the accreting companion and rotating in the reference frame of the binary system. Most of the simulations were run on a grid with 128 radial zones times 384 angular zones and 3 additional levels of refinement. The radial spacing in our base grid is uniform. Fig. 3 shows a diagram of the grid geometry and boundaries in the RLOF setup. The computational grid was centered on the accretor and a stream is initially introduced over a few cells at the inner Lagrangian point. Some tests were run with twice the linear resolution to check the convergence of the results (see Sect. 4.2.4).

Two different equations of state were used in our model. One version uses an isothermal Riemann solver and the adiabatic models use an ideal gas equation of state with polytropic index γ in the range 1 to 5/3. The isothermal code was used to explore the parameter space because of its relative speed without the need to calculate the cooling and heating terms and evolving the energy equation.

3.4. Wind accretion

In this section we describe our numerical setup to study wind accretion in detached symbiotic binaries where the AGB component does not fill its Roche lobe. Many detached interacting binaries, including symbiotic binaries and X-ray binaries show evidence for much higher mass transfer rate than predicted by models of spherically symmetric wind. The enhanced accretion rates onto the secondary can be explained by wind focused towards the compact companion.

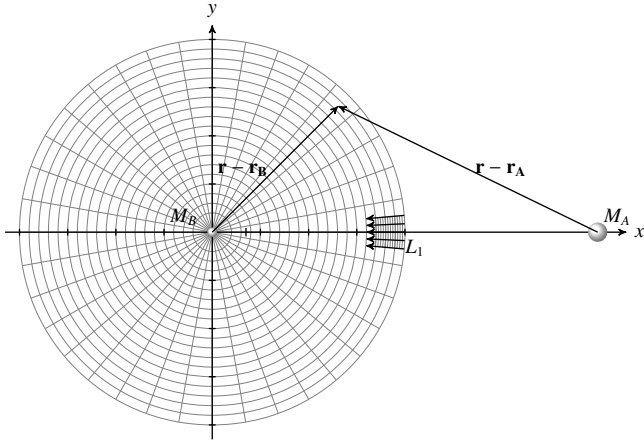


FIG. 3.— Grid geometry of the RLOF simulations in polar coordinates. The computational domain is centered on the accretor and a stream introduced over a few cells at the inner Lagrangian points.

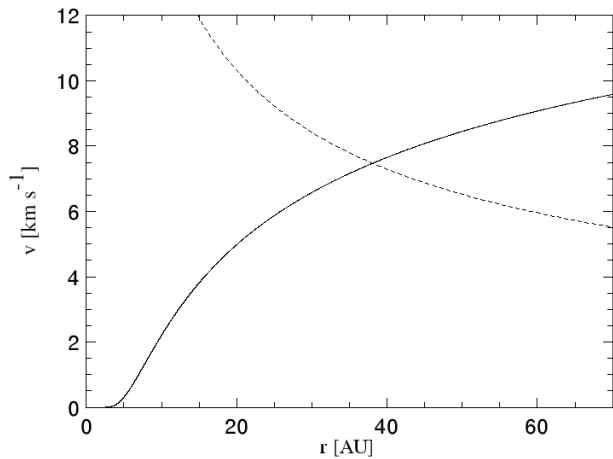


FIG. 4.— Radial velocity profile of the unperturbed wind for a temperature of 10^3 K. The dotted line corresponds to the escape velocity from a $1.2M_{\odot}$ star.

3.4.1. Wind model

The initial spherically symmetric wind structure is obtained by solving the momentum equation

$$v_r \frac{dv_r}{dr} + \frac{1}{\rho} \frac{dP}{dr} = -\frac{GM_A}{r^2}, \quad (18)$$

where v_r is the radial component of the wind velocity and M_A the mass of the central star. The solution for an isothermal wind is shown in Fig. 4. As the wind propagates across the grid it is accelerated by thermal pressure and its velocity increases. It is possible that AGB winds are not completely spherically symmetric due to internal processes in the star or the influence of the secondary (Dorfi & Hoefner 1996).

In Fig. 5 we plot the temperature profile used in our wind model. During the AGB phase it is likely that the winds are primarily radial since the massive stellar atmosphere cannot have significant rotation. Our temperature distribution has a radial profile $\propto r^{-0.5}$ and is similar to the one given by the AGB models by Ivezić & Elitzur (1997). Fig. 9 shows the temperature distribution after 6 orbits in our locally isothermal simulations.

The binary systems considered here consist of a $1.2M_{\odot}$

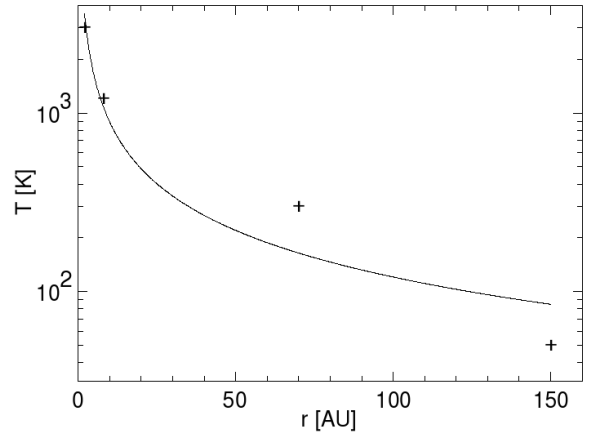


FIG. 5.— Temperature as a function of distance from the AGB star in logarithmic scale used in our calculations for different wind acceleration radii. The temperature is $\sim 10^3$ K at 10 AU where dust is formed. The crosses give dust temperature estimates from IR observations of the symbiotic system Mira AB (Marengo et al. 2001).

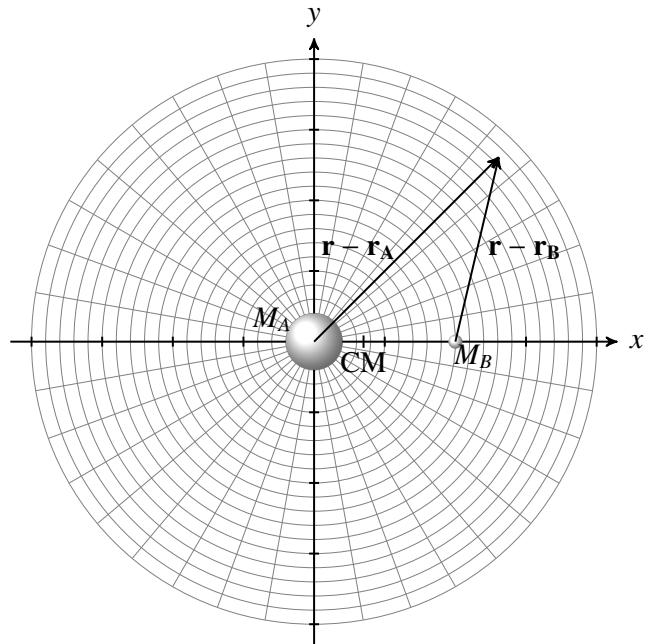


FIG. 6.— Schematic representation of the grid geometry in polar coordinates. The physical quantities are defined in the center of the cells. The system is centered on the primary and rotating in clockwise direction.

AGB star and a $0.6M_{\odot}$ companion. The orbital separation d ranges between 10 AU and 70 AU. The initial temperature of the wind is between 3000 K and 10000 K and the velocity of the wind on the surface of the AGB star is $2 - 15 \text{ km s}^{-1}$. Both temperature and the radial velocity of the wind are constant at the dust formation radius for a given wind model.

The computational domain was centered on the primary and the secondary was fixed on a circular orbit neglecting the hydrodynamic effects. Our grid extended out to twice the binary separation in our models which is enough to avoid mass loss from the disk around secondary. We used a grid with a fixed uniform size in the radial and azimuthal directions. The grid cells were sized to give square cells at the location of the secondary's orbit. To improve the resolution close to the sec-

ondary additional levels of refinement were used to speed up the simulation. We introduce the mass of the secondary over 1 orbital period to avoid the formation of strong shocks. The adaptive mesh refinement allows us to resolve a broad range of density contrasts close to the secondary. A diagram of the grid geometry is shown in Fig. 6.

We assume that the wind is driven by radiation pressure and is composed of dust and a photoionized ideal monoatomic gas which are perfectly coupled. The wind acceleration mechanism is not considered in our model. The wind is accelerated at the dust condensation radius according to the Eq. 18 where the full gravity of the AGB star is included. We include gas forces due to pressure and gravity from the AGB and the compact companion but the self-gravity of the gas is neglected. In our adiabatic runs, we assume that the gravity of the red giant is balanced by radiation pressure on the dust, so that it does not appear explicitly in our equations. Dust grains form in the AGB envelope, where pulsational shocks bring material from the atmosphere, and deposit it in the region of ~ 2 photospheric radii. In this case the only force acting on the wind from the AGB star is the gas pressure, whereas in a binary the wind is additionally subject to the gravity of the companion. Such an approximation leads to terminal velocities of the wind ranging between $10 - 40 \text{ km s}^{-1}$, comparable to those obtained by Winters et al. (2000) for winds in which radiation pressure nearly balances the gravity of the wind source (see e.g. Gawryszczak et al. 2002). The effects of cooling are accounted for by a nearly isothermal equation of state in some of our runs, while in the adiabatic runs the polytropic index γ is in the range $1 - 5/3$.

We neglect radiation pressure from the secondary. In the case of a white dwarf companion, for typical dust grain sizes the effect of radiation pressure on grains is negligible compared with gravity focusing. Explicit radiative heating or cooling terms are also neglected in our wind model.

3.4.2. Equation of state

The pressure is obtained by

$$p = \frac{\mathcal{R}\rho T}{\mu}, \quad (19)$$

where \mathcal{R} is the gas constant, T is the temperature and μ is the mean atomic weight.

The temperature is approximately constant at the secondary's position. Because of the gravitational field of the accretor, the disk aspect ratio calculated with respect to the $h_B = H/|\mathbf{r} - \mathbf{r}_B|$ can decrease considerably. This influences the flow in vicinity of the secondary and increases the amount of gas accumulated inside the Hill sphere. On the other hand we should expect a temperature increase in the vicinity of the secondary. For of a permanent disk h_B can increase due to the compression of the gas flowing into the vicinity of the accretor. We use the following expression to calculate the sound speed

$$c_s = \frac{h_A r_A h_B r_B}{((h_A r_A)^n + (h_B r_B)^n)^{1/n}} \sqrt{\frac{GM_A}{r_A^3} + \frac{GM_B}{r_B^3}}, \quad (20)$$

where $r_A = |\mathbf{r} - \mathbf{r}_A|$ is the distance from the mass-losing primary, $r_B = |\mathbf{r} - \mathbf{r}_B|$ is the distance from the secondary, and a parameter $n = 2$ is used in our simulations.

A disk with constant aspect ratio h_B can be formed around

TABLE 1
MODEL PARAMETERS OF A LONG-PERIOD AND CLOSE SYMBIOTIC BINARIES.

Parameter	long-period	short-period
Mass of primary M_A (g)	2.387×10^{33}	2.387×10^{33}
Mass of secondary M_B (g)	1.193×10^{33}	1.193×10^{33}
Radius of primary R_A (cm)	2.394×10^{14}	2.394×10^{14}
Radius of secondary R_B (cm)	1.496×10^{14}	1.496×10^{14}
Wind temperature T_{wind} (K)	1000	1200
Binary separation d (cm)	1.047×10^{15}	2.394×10^{14}
Period P_b (yr)	436.5	40.9

the mass gainer with a Keplerian angular velocity

$$\Omega_B = \sqrt{\frac{GM_B}{r_B^3}}. \quad (21)$$

3.4.3. Model parameters

The main parameters of the models are the wind temperature that determines its terminal velocity, the orbital parameters (binary separation and orbital period for a circular orbit), mass loss rate from the AGB star and the mass ratio defined by

$$q = \frac{M_A}{M_B}, \quad (22)$$

where M_A is the mass of the primary mass-losing star and M_B is the mass of the wind-accreting compact star.

Here we describe the model parameters of the runs discussed in Section 4. The indexing of the models described below increases with increasing dust condensation radius to facilitate reference to models. The average wind terminal velocity from an AGB star is around 15 km s^{-1} , within a range of 10 km s^{-1} . In the following, we produce models having a terminal velocity for a single star between 10 and 25 km s^{-1} . The binary separations d vary between 10 and 70 AU . Our base resolution with 3 levels of refinement corresponds to a cell size of ~ 0.004 close to the accretor. Each simulation with our standard resolution requires about 30 hours of CPU time on Pentium 4 processors.

The inner Lagrangian point in model M-4 is at 40 AU from the mass-losing star, which is close to the inner boundary of the domain. In this case we expect to see some of the effects of RLOF in addition to that of wind accretion.

The parameters in these simulations are closely related to two symbiotic systems Mira AB and R Aqr (see Table 1). The wide symbiotic system Mira AB (α Ceti) consists of a pulsating AGB primary (Mira) and a compact secondary at an *Hip-parcus* distance of $\sim 128 \text{ pc}$. Mira stars are long-period variable stars which evolve along the AGB and present large stellar pulsations. The primary's radius is found to be $\sim 270 R_\odot$. The nature of the companion is uncertain and has been suggested to be a white dwarf or a late-type, magnetically active main-sequence dwarf. HST observations of Mira AB have shown that it is a strongly interacting system with mass transfer from the primary towards the compact companion. Its optical through UV spectrum appears to be dominated by emission from an accretion disk that presumably is accumulated from Mira A's massive wind (Reimers & Cassatella 1985; Karovska et al. 1997). Recent observations of symbiotic binaries in wavebands ranging from the IR to the X-rays suggest that wind focusing can form a stream flow even in wide systems (Karovska et al. 1997, 2005). The system has large variations in luminosity with well-defined pulsation periods.

X-rays from the Mira AB system arise either from magnetospheric accretion of wind material from Mira A onto Mira B, or from coronal activity associated with Mira B itself, as a consequence of accretion-driven spin-up.

R Aqr is a close symbiotic binary system (at a distance of ~ 200 pc) composed of a mass-losing Mira variable and a white dwarf surrounded by an extended nebula (Solf & Ulrich 1985). The orbital period is not well determined with values in the literature ranging between 20 and 44 yr (Willson et al. 1981; Hinkle et al. 1989; McIntosh & Rustan 2007). The companion is surrounded by an accretion disk which gives rise to a jet with bipolar outflow. The primary almost fills its Roche lobe during periastron, although mass flow towards the companion is increased due to wind focusing during the rest of the orbital motion (Gromadzki & Mikolajewska 2008).

4. RESULTS AND DISCUSSION

The wind parameters and mass ratio of our models of wind accreting symbiotic binaries are given in Table 2. We will consider mainly the simulations with a locally isothermal equation of state in the following discussion. The adiabatic runs will be considered in Sec. 4.2.2.

4.1. Roche lobe overflow

First, we study the accretion in the RLOF case to check our code and compare the results with the wind accreting cases described below in Sec. 4.2. Also, in some symbiotics RLOF is likely to occur during periastron if their orbits are highly elliptical, for example in R Aqr where the stellar separation becomes 8 AU (Gromadzki & Mikolajewska 2008). The gas from the primary star is assumed to flow through the inner equilibrium point with an initial velocity between 0.01 – 0.1 of the orbital velocity. We run our simulations for 5 orbital periods, when the system has reached a quasi-steady state.

Our simulations show that most of the flow is efficiently accreted onto the star as it turns around and forms a stable disk with counterclockwise rotation and elliptic streamlines. The gas is accelerated by the companion’s gravity and Coriolis force and becomes supersonic. The L_1 stream cannot hit the companion star due to the Coriolis force and penetrates into the disk forming a hot spot that heats up the outer disk in our adiabatic runs with $\gamma = 5/3$.

In Fig. 7 we show the density contours for a system with separation of 70AU and L_1 Lagrangian point located at ~ 30 AU from the accretor using two different equations of state. Mass is removed inside 0.5 Hill radius in our simulations to achieve a quasi-stable state after several orbital periods. The angle of deflection of the stream roughly agrees with the analytical estimates of Lubow & Shu (1975). Fig. 8 shows the velocity vectors in the inertial frame for one of the RLOF runs.

The flow patterns are non-axisymmetric due to the shock waves that form when gas rotating in the disk collide with the stream. This kind of patterns have been observed using Doppler tomography in the disk around IP Pegasi (Steeghs et al. 1997; Makita et al. 2000). The angular momentum transfer in the disk is more efficient due to the presence of shocks and accretion may take place without turbulent viscosity. There is some mass loss in our grid in the case of reflective boundaries at the accretor’s surface.

Since cooling effects due to radiation are not included in our equation of state we use a locally isothermal model where the temperature decreases as r^{-1} from the center of the secondary. In this case the stream shocks are stronger than in the adiabatic runs (right panel in Fig. 7).

TABLE 2
MODELS WITH SEPARATION 70 AU AND MASS RATIO $q = 2$ FOR DIFFERENT DUST FORMATION RADIUS.

Model	Dust formation radius (AU)	Wind temperature (K)	q	h_B
M-1	10	900	2	0.1
M-2	20	490	2	0.1
M-3	30	340	2	0.1
M-4	40	300	2	0.1
M-5	30	300	2	0.05

4.2. Wind accretion

Our results indicate that wind accretion in symbiotic binaries can result in RLOF-like accretion via a stream flow. Stable accretion disks can form for winds with mass loss ranging between $10^{-9} - 10^{-6} M_{\odot} \text{yr}^{-1}$ (Ryde et al. 2000) and distances between 16 – 70AU.

The mass accretion rates onto the secondary are of the order of the predicted ones from Bondi-Hoyle theory when the inner boundary of our grid is less than 20AU. Here, we will focus on slow winds with a relative speed at the position of the accretor of 6 – 25km s^{-1} . Mass accretion ratios for different values of the accretion radius r_{acc} inside the Hill radius in Eq. 15 give very similar results after we reach a stable configuration. In our runs with 4 additional levels of refinement around the accretor, the accretion ratio is consistent with the lower resolution simulations.

For a fast wind we expect an accretion rate of the order of the Bondi-Hoyle accretion (Bondi & Hoyle 1944). In this case we find a quasi-spherical wind morphology. For wind acceleration radii between 30 to 40AU the accretion rate is a few times the Bondi-Hoyle rate with variations with an amplitude of about 10%. The wind presents a broad range of density contrasts in our computational domain. Bow shocks are formed close to the secondary in these models at late times. It has been suggested that UV radiation in symbiotic systems is originated in those shocks (Theuns & Jorissen 1993). In Table 2 we show the parameters of our models that reproduce closely the binary system Mira AB for different wind acceleration radii. For typical mass loss rates from an AGB star (Ryde et al. 2000) we compute an accretion rate on the companion of $\sim 10^{-7} - 10^{-9} M_{\odot} \text{yr}^{-1}$ via stream flow accretion. The X-ray luminosity of the accretor can be estimated using

$$L_X = \frac{GM_{\text{acc}}M_B}{R_B}, \quad (23)$$

which corresponds to $\sim 3 \times 10^{30} - 3 \times 10^{32} \text{erg s}^{-1}$, assuming a radius $R_B = 0.02R_{\odot}$ for the compact object in our M-3 model. In Fig. 12 we compare the accretion ratio in our models with the Bondi-Hoyle accretion given by Eq. 3. Table 3 shows accretion rates onto the compact object divided by the mass loss rate of the AGB star as a function of time. Accretion ratios become quasi-stable after half of an orbit of the system. However, in the Bondi-Hoyle formula the velocity is the upstream wind velocity at infinity, while in our binary simulations we use the relative wind velocity at the secondary position. Moreover, the plane parallel flow assumption in the Bondi-Hoyle theory is not valid for our wind model at close distances.

A small change in the wind parameters can lead to changes of a few times in the accretion rate when an accretion disk is formed around the secondary. In particular, it could explain the increase of extinction in symbiotic binaries (Gromadzki &

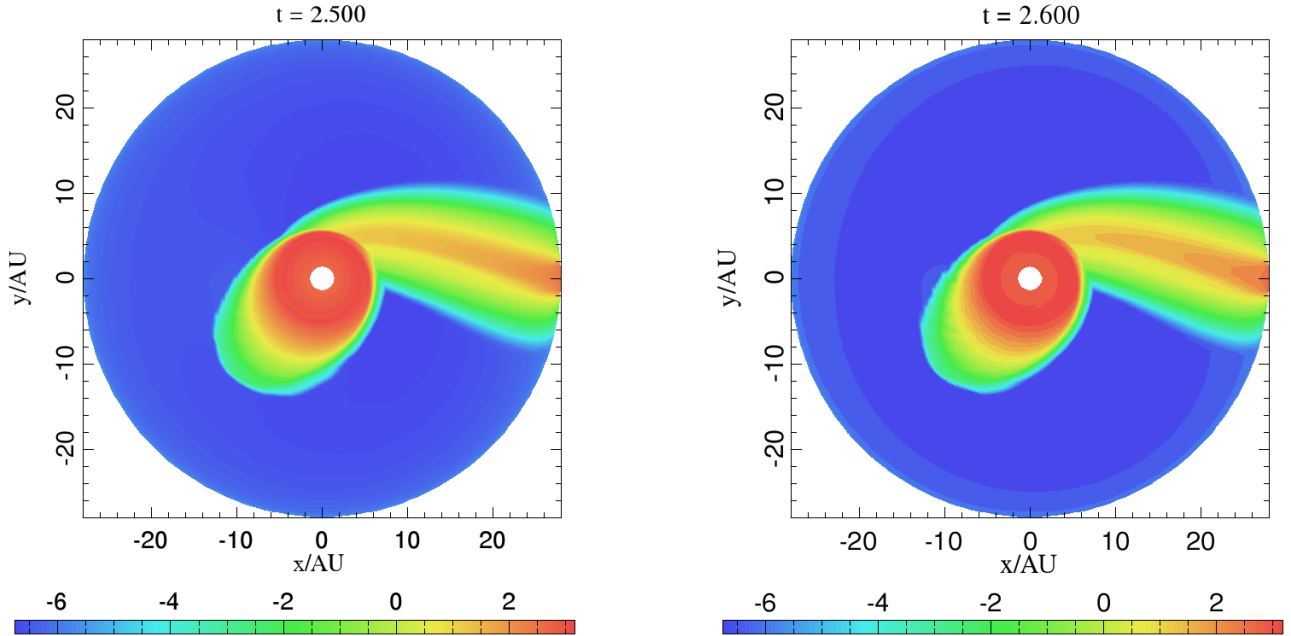


FIG. 7.— Density contours in the orbital plane of an RLOF simulation for an adiabatic run with $\gamma = 1.1$ (left) and a locally isothermal run (right). The system has a separation of 70AU and a mass ratio $q = 2$.

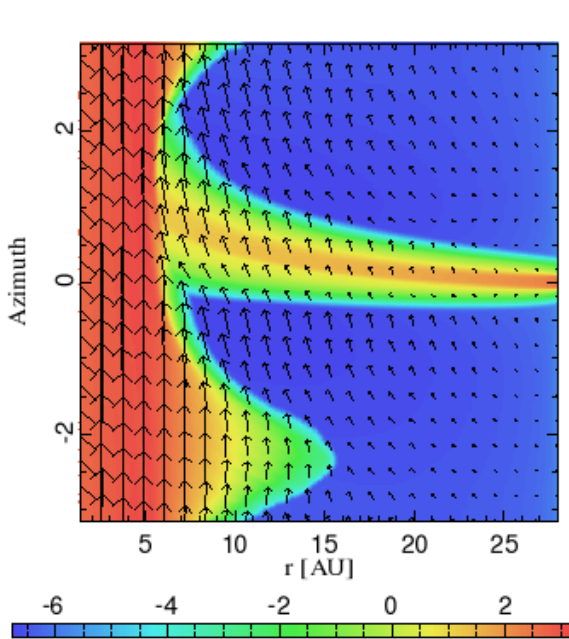


FIG. 8.— Density contours in the orbital plane in polar coordinates for the RLOF simulations after 1 orbit. Velocity vectors are shown in the inertial frame.

Mikolajewska 2008) as a change in the accretion flow. Those variations can occur in a fraction of the orbital period and may also explain Nova outbursts in objects such as RS Ophiuchi (Walder et al. 2008).

In Fig. 13 the azimuthally averaged density distribution close to the accreting star for model M-3 is shown. The density decreases exponentially up to 5 AU in a slightly eccentric disk and is likely to be optically thick. This is consistent with the size of the disk around Mira B estimated by Ireland

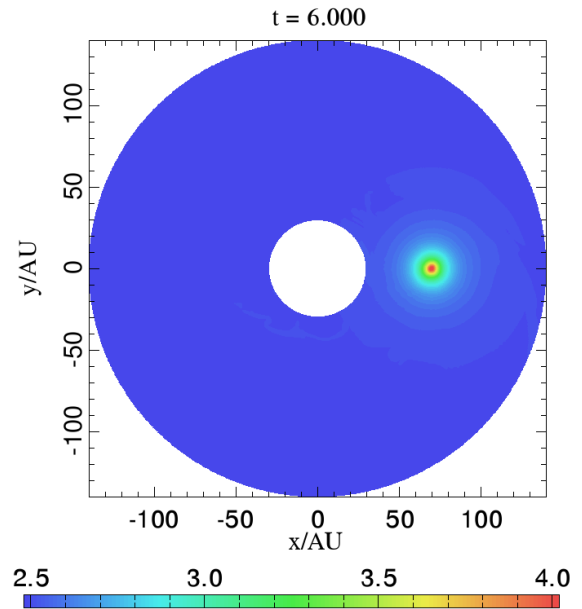


FIG. 9.— Temperature distribution in logarithmic scale after 6 orbits for a binary system with separation of 70AU.

et al. (2007). We show the flowlines after 1 orbital period in Fig. 14. The flowlines are calculated integrating the equation of motion from the line joining the stars using positive and negative time-steps. When the wind speed is of the order of the escape velocity from the AGB star the flow is focused by the gravitational pull from the secondary and the accretion rate is enhanced by a factor of a few with respect to standard Bondi-Hoyle accretion.

We show the radial velocity map for a model with wind temperature 10^3 K and inner boundary at 20 AU with over-

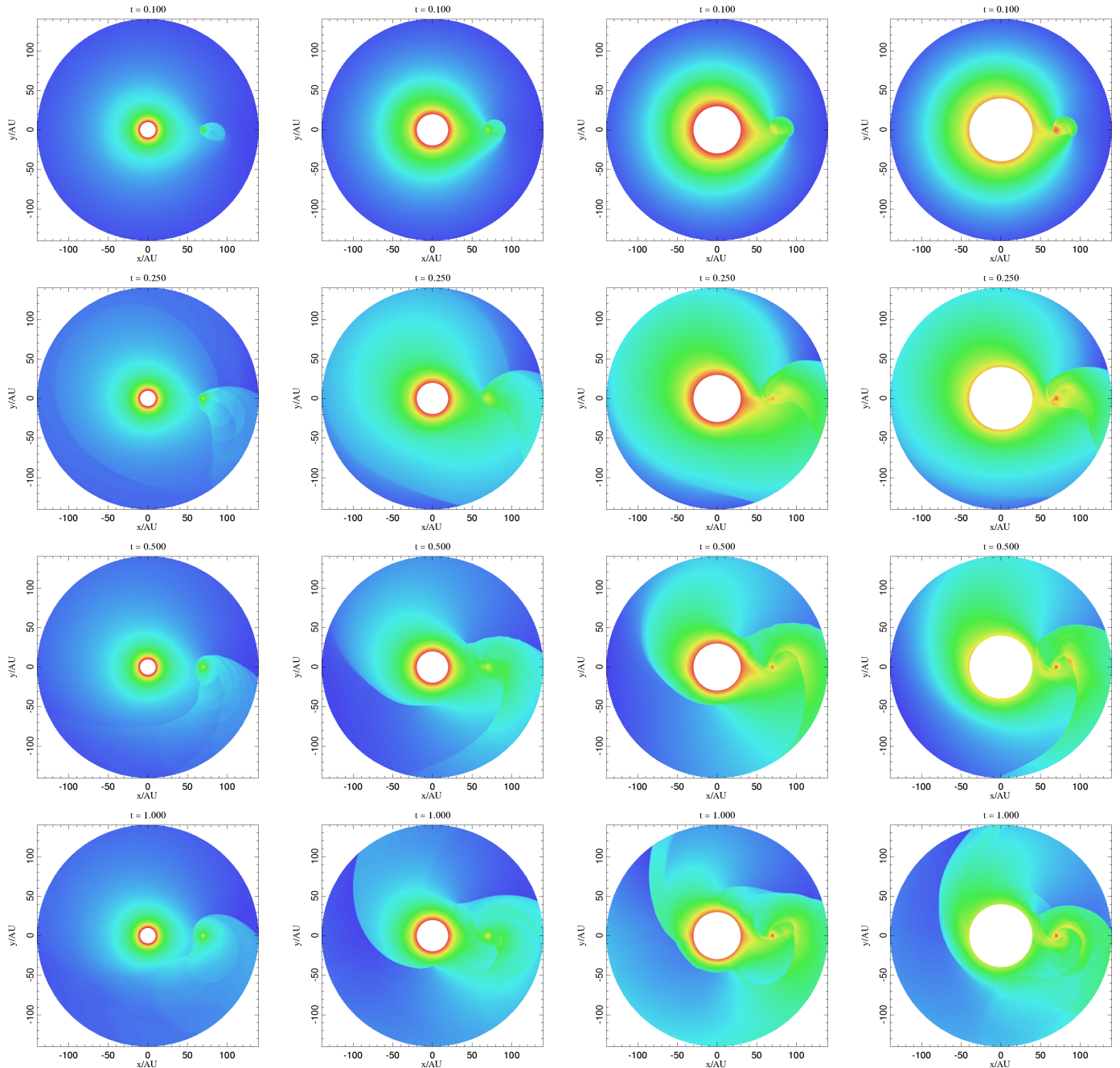


Fig. 10.— Density contours in logarithmic scale for a separation of 70AU at several times. From left to right the inner boundary where the wind is accelerated is 10, 20, 30 and 40AU. The model parameters are presented in Table 2. In the outermost right column the envelope of the primary is close to the Hill surface. Three snapshots are shown for times $t = 0.25, 0.5$ and 1 orbital periods. The temperature of the wind decreases roughly as r^{-1} where r is the distance from the primary.

plotted grid structure in Fig. 15. The refinement criterion used by PARAMESH is based on the second derivative normalized by the gradient over one cell (Löhner 1987). The blocks are approximately square close to the secondary and contain 8×8 computational cells.

The orbital speed in the disk is close to Keplerian with a steeper radial profile. In Fig. 16, we plot the averaged azimuthal velocity around the secondary.

4.2.1. Influence of the wind temperature

We tried several models to check the dependence of the wind parameters on the formation of a stream flow between

the stars. The dust is believed to be condensed at a temperature of $\sim 1500\text{K}$ which corresponds to a distance of 8 AU from the center of the primary (Ivezic & Elitzur 1997). When the wind acceleration radius is of the order 50% of the Hill radius a density enhancement is formed focusing 10% of the slow wind inside the Roche lobe. The sound speeds in our models are in the range $3 - 10\text{km s}^{-1}$ which are of the same order of the wind speed relative to the accretor. When the average velocity of the wind at the inner Lagrangian point is larger than the orbital velocity of the system, the stream does not form and the accretion ratio is close to Bondi-Hoyle estimate.

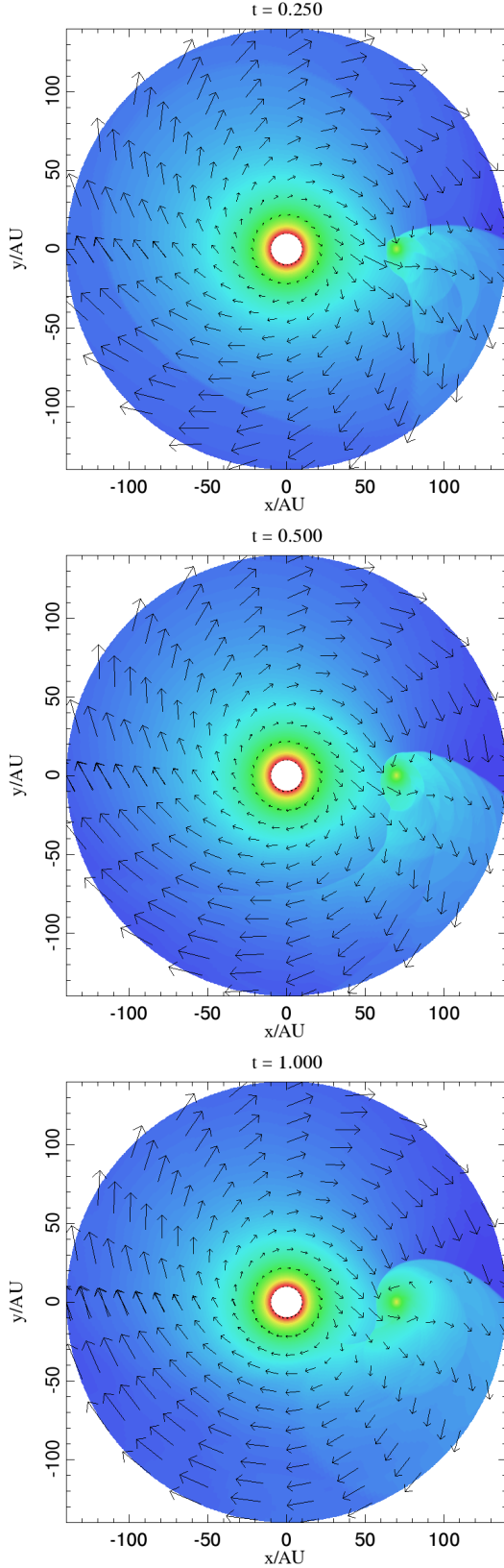


FIG. 11.— Density maps and velocity vectors in the orbital plane in logarithmic scale for a separation of 70AU. Three snapshots are shown for times $t = 0.5, 1$ and 1.5 periods after the secondary is introduced.

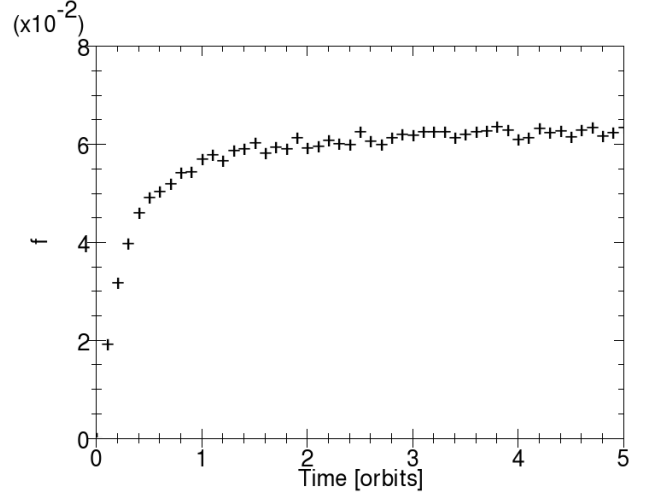


FIG. 12.— Accretion ratio, defined as the accretion rate divided by the mass-loss rate from the AGB star, as a function of time for our model M-5 (see Table 2).

TABLE 3

ACCRETION RATIOS AS A FUNCTION OF TIME FOR THE SIMULATION SHOWN IN FIG. 12.

Time (orbits)	$\frac{M_{\text{acc}}}{M_{\text{wind}}}$
0.1	0.0187499146615
0.2	0.032895734525
0.3	0.0405163717933
0.4	0.0457114513595
0.5	0.0486647436321
0.6	0.052120162122
0.7	0.0518595175058
0.8	0.0545558407777
0.9	0.0543526731365
1.0	0.0550009176397
1.1	0.0557649810422
1.2	0.0573139141097
1.3	0.0579923479442
1.4	0.0587394563781
1.5	0.0588350261856
1.6	0.058462177135
1.7	0.059570725981
1.8	0.0612462210888
1.9	0.0612788117294
2.0	0.0605904603547

In Fig. 10, we show the density contours for a binary separation of 70AU for several values of the dust formation radius where the wind is accelerated. In these simulations we include the full gravity of the primary.

For a dust formation radius of 5AU the wind geometry is almost spherical. A bow shock forms as the wind is decelerated by the gravity from the companion and the accretion ratio is close to the Bondi-Hoyle value. A small accretion disk is formed around the secondary. As we move the dust formation radius outwards the temperature for dust condensation decreases according to Fig 5. When we place the dust formation radius at 10AU the flow structure is clearly elongated and the accretion rates are a few times larger than the Bondi-Hoyle theoretical estimate. This is consistent with an agglomeration of dust particles at several stellar radii above the photosphere in AGB stars in order to have focused wind RLOF-like mass transfer via stream flow in wide symbiotic systems such as Mira AB (Karovska et al. 2005).

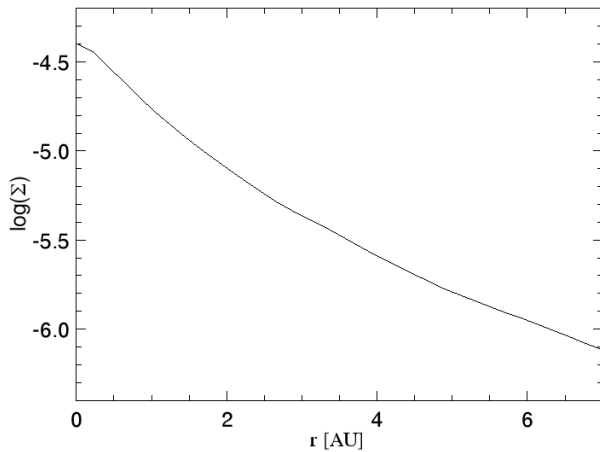


FIG. 13.— Averaged radial density profile of the disk around the accreting secondary in logarithmic scale in computational units after 1 orbit for the model shown in Fig. 11. The distance in the horizontal axis is given in AU from the center of the secondary.

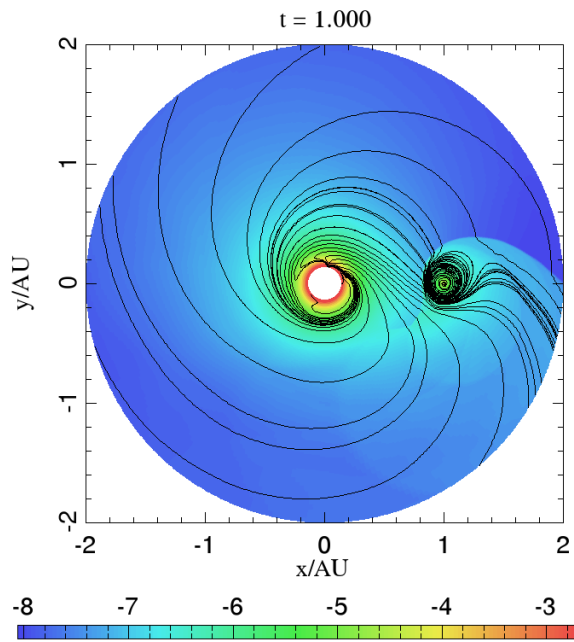


FIG. 14.— Streamlines in the corotating frame after 1 orbit overlaid on the density contours in logarithmic scale for the same model as shown in Fig. 11. The flowlines around the secondary are eccentric.

For the cases where the dust formation is ≤ 20 AU the wind velocity is lower than the escape velocity in our model. The wind opposite from the companion is not able to overcome the gravity and forms a bow shock. This does not affect the formation of a tidal stream and our calculation of the mass accretion rate onto the secondary. The escape velocity from the primary is $\sim 10 \text{ km s}^{-1}$ at the dust formation location in our model M-2 (second column in Fig. 10). In the slow wind case, numerical simulations show intricate flow patterns, therefore it is not possible to apply directly the results from Bondi-Hoyle accretion theory.

In our model M-5, we have changed the temperature profile around the secondary. The accretion ratios averaged over one

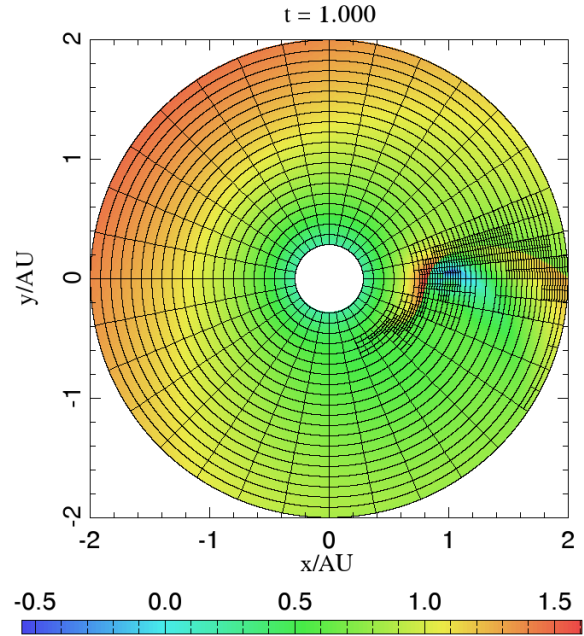


FIG. 15.— Radial velocity contours in the corotating frame after 0.5 orbits with grid structure using 3 levels of refinement. Each block has 8×8 computational zones.

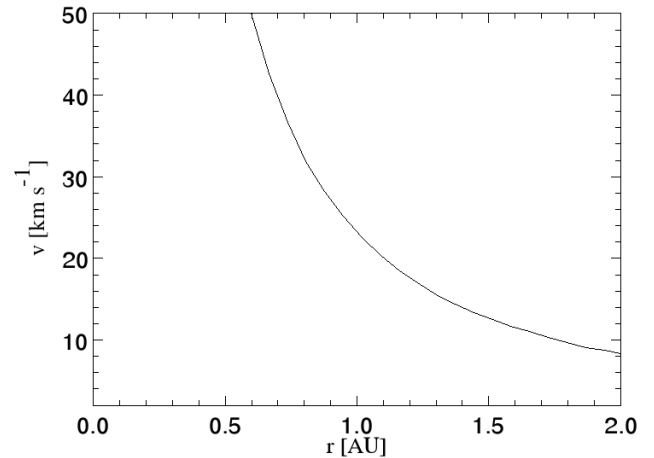


FIG. 16.— Averaged orbital velocity profile of the accretion disk around the secondary for the model shown in Fig. 11. The distance in the horizontal axis is given in AU from the center of the secondary.

orbital period agree within 5% in our models M-3 and M-5.

4.2.2. Modifying γ

We have varied the polytropic index between $\gamma = 1 - 5/3$. The density distributions are similar within 10% for the simulations with $q = 2$, $d = 70 \text{ AU}$ and $\gamma = 1, 1.2, 5/3$. The variation of the polytropic index intends to bracket more realistic cases that include radiative losses in the equation of state. In the adiabatic simulations the accretion ratio varies between 8 – 10% and is several times larger than in the Bondi-Hoyle scenario.

4.2.3. Variation of the orbital parameters

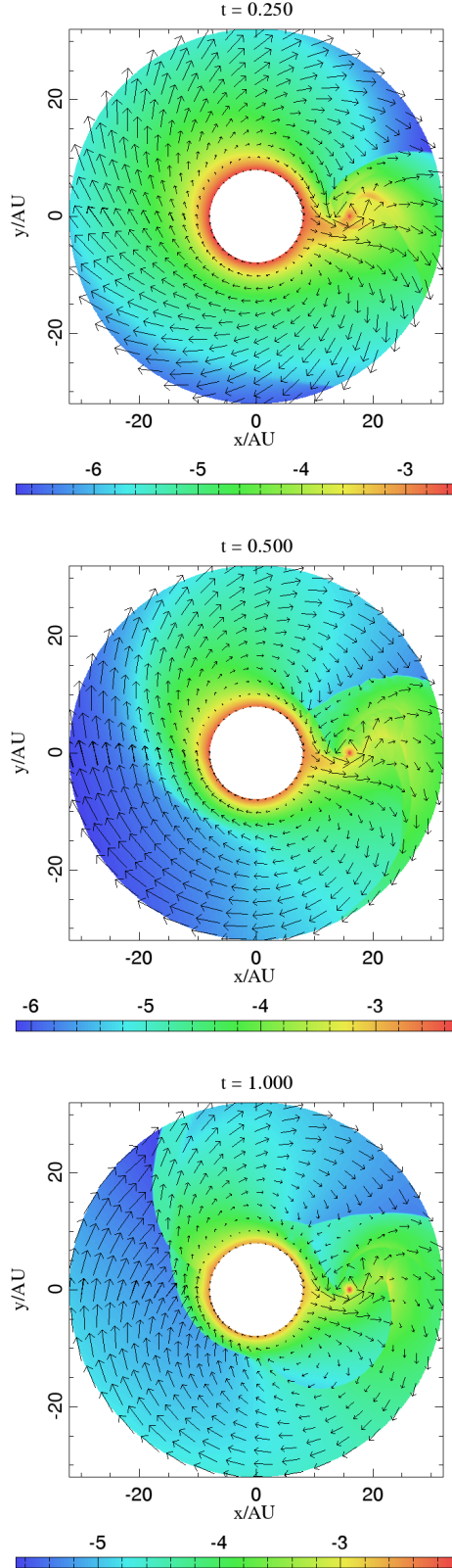


FIG. 17.— Density contours in the orbital plane with overplotted velocity vectors in the corotating frame for a system with separation of 16AU after 0.25, 0.5 and 1 orbital periods.

The orbital velocity in our models varies between $5 - 10 \text{ km s}^{-1}$ while the wind velocity at the surface of the AGB is of the order $2 - 10 \text{ km s}^{-1}$.

In Fig. 17 the density contours of a system with separation of 16AU and mass-losing surface located at 8AU from the origin is shown as a function of time. The central star has a mass of $1.2M_{\odot}$ and an accreting companion of $0.6M_{\odot}$ orbits on a fixed circular orbit. An accretion disk is observed around the secondary with Keplerian velocity profile and a narrow stream forms between the stars. The accretion flow focused onto the secondary is about 15% of the unperturbed wind mass loss which is several times more efficient than the models for binary separation of 70AU. Mass is removed from the accretion disk after each time-step to avoid the accumulation of mass and formation of strong shocks according to Eq. 15 (Günther & Kley 2002).

4.2.4. Convergence tests

We have rerun simulation M-3 at a twice the linear resolution of our reference simulations with three levels of refinement, and performed an additional run at the same base resolution with four additional levels of refinement. In our high resolution runs, the gravitational softening ϵ is half the size of the gravitational softening in the low resolution runs. The density distributions in the higher resolution simulations agree with our previous results within 5% with larger oscillations. Therefore, we conclude that the resolution of our simulations is acceptable and does not affect our results.

5. CONCLUSIONS

We have constructed a hydrodynamical time-dependent model of a wind from an AGB star which is gravitationally focused by a close companion. The model has several free parameters. The mass ratio q of the system, the binary separation d and the eccentricity e characterize the binary configuration. The effective temperature on the surface of the mass losing star, the radius of the AGB star where the dust is formed and the mass loss describe the properties of the wind from the mass-losing star. We have improved on previous hydrodynamic simulations by using an equation of state where the temperature distribution depends on the distance from the primary star and the accreting companion.

For each binary model we integrate the equations of hydrodynamics until the density distribution of the gravitationally focused wind reaches a stationary state. The general effect of the secondary is to deflect the AGB wind toward the orbital plane, and as a result the relaxed density distributions present accretion disks of various characteristics. Accretion via a gravitationally focused wind has implications for a broad range of symbiotic and wide binary systems and can explain the formation of chemically peculiar stars. A tidal stream is observed in our runs for binary separations up to $\sim 70 \text{ AU}$ for slow winds and nearly isothermal flows. Wind focusing weakens with increasing orbital separation because of the increasing ratio of the wind velocity at the secondary's position to the orbital velocity of the system.

All our models develop a high density region in the form of a Keplerian thin disk around the secondary with a mass of about $10^{-4}M_{\odot}$ and an exponentially decreasing density profile. The temperature profile around the accretor was fixed in our simulations and corresponds to a disk scale height of ~ 0.05 . Winds from evolved stars in binary systems show complex flow patterns and are far from being spherically symmetric. A thin accretion disk around Mira B has been inferred

from spectroscopic UV observations (e.g. Reimers & Cassatella 1985; Karovska et al. 1997) and interferometric imaging (Ireland et al. 2007). The formation of a stream flow is strongly dependent on the wind temperature at the dust formation radius which determines the wind velocity at the inner Lagrangian point. For the winds parameters from a AGB star (Mira type) we obtain stable disks with masses of the order 10^{-4} of the stellar mass for a range of orbital separations. The accretion rate onto the secondary is almost constant once the accretion disk is formed and we reach a quasi-stable state. We conclude that the main parameter that determines the formation of a stream and enhanced accretion rates compared to Bondi-Hoyle's rates is the wind velocity at the dust formation radius. Nevertheless, the Bondi-Hoyle estimate does not include pressure forces and is not directly applicable to our models of wind accretion in symbiotic binaries.

The presence of a long-lived disk and stream flow is sensitive to the wind parameters, in particular of the dust acceleration radius where we place the inner boundary of our grid. In case that the wind parameters change with time the accretion rates can be expected to change in relatively short time-scales due to rapid changes in the flow patterns and the formation of a stream flow. This can explain the variability in accretion rate and transitions from a quiescent to an active state in binary systems (Bisikalo et al. 2002). As the secondary increases in mass there are several possible outcomes for the system. The angular momentum loss in symbiotic binaries may be large enough to imply a shrinking of the orbit and a possible merger that can lead to the formation of Barium stars or Type Ia supernovae (Theuns et al. 1996; Jahanara et al. 2005).

The massive wind of an AGB star can be considerably deflected towards the orbital plane by the gravitational interaction with a companion star. The X-ray luminosity powered by accretion onto the mass gainer can photoionize the wind and reduce its ability to be accelerated by radiation pressure. The

lower radiative driving can result in a reduced wind velocity near the companion, which further increases the the accretion efficiency of the companion. In the case of rapid accretion rate changes a symbiotic binary may undergo outbursts such as those observed in Mira AB (Karovska et al. 2005). A detailed comparison of the results from the numerical models with multi-wavelength observations of Mira AB will be presented elsewhere.

We have adopted a simple a simple prescription for the equation of state and wind acceleration mechanism. In the future our calculations can be improved by using a more detailed energy balance for the gas going beyond the isothermal approximation including radiation cooling and heating due to shock formation. Radiative feedback is also expected to be important in the context of symbiotic systems and X-ray binaries (Edgar & Clarke 2004). We plan to perform 3-dimensional simulations to compare our numerical results with high resolution X-ray observations of the Mira AB system.

MdVB was supported by a SAO predoctoral fellowship during the course of this work. MK is a member of the Chandra X-ray Center, which is operated by the Smithsonian Astrophysical Observatory under NASA contract NAS8-03060. The FLASH code used in this work is developed in part by the U.S. Department of Energy under Grant No. B523820 to the Center for Astrophysical Thermonuclear Flashes at the University of Chicago. Some of the simulations reported here were performed at the Center for Parallel Astrophysical Computing operated by the Institute for Theory and Computation at the Harvard-Smithsonian Center for Astrophysics. MdVB thanks P. Artymowicz for valuable discussions. We would like to thank the anonymous referee for helpful comments and suggestions.

REFERENCES

- Arndt, T. U., Fleischer, A. J., & Sedlmayr, E. 1997, *A&A*, 327, 614
 Bisikalo, D. V., Boyarchuk, A. A., Kilpio, E. Y., & Kuznetsov, O. A. 2002, *Astronomy Reports*, 46, 1022
 Blackman, E. G., Frank, A., Markiel, J. A., Thomas, J. H., & Van Horn, H. M. 2001, *Nature*, 409, 485, arXiv:astro-ph/0101492
 Bondi, H. 1952, *MNRAS*, 112, 195
 Bondi, H., & Hoyle, F. 1944, *MNRAS*, 104, 273
 Bowen, G. H. 1988, *ApJ*, 329, 299
 Bowen, G. H., & Willson, L. A. 1991, *ApJ*, 375, L53
 Calder, A. C. et al. 2002, *ApJS*, 143, 201, arXiv:astro-ph/0206251
 Colella, P., & Woodward, P. 1984, *J. Comput. Phys.*, 54, 174
 de Val-Borro, M., Artymowicz, P., D'Angelo, G., & Peplinski, A. 2007, *A&A*, 471, 1043, arXiv:0706.3200
 de Val-Borro, M. et al. 2006, *MNRAS*, 370, 529, arXiv:astro-ph/0605237
 Dorfi, E. A., & Hoefner, S. 1996, *A&A*, 313, 605
 Edgar, R. 2004, *New Astronomy Review*, 48, 843, arXiv:astro-ph/0406166
 Edgar, R., & Clarke, C. 2004, *MNRAS*, 349, 678, arXiv:astro-ph/0312325
 Freytag, B., & Höfner, S. 2008, *A&A*, 483, 571
 Fryxell, B. et al. 2000, *ApJS*, 131, 273
 García-Segura, G., & López, J. A. 2000, *ApJ*, 544, 336, arXiv:astro-ph/0007189
 García-Segura, G., López, J. A., & Franco, J. 2001, *ApJ*, 560, 928
 Gawryszczak, A. J., Mikołajewska, J., & Różyczka, M. 2002, *A&A*, 385, 205
 González, R. F., de Gouveia Dal Pino, E. M., Raga, A. C., & Velazquez, P. F. 2004, *ApJ*, 600, L59, arXiv:astro-ph/0310010
 Gromadzki, M., & Mikołajewska, J. 2008, *ArXiv e-prints*, 804, 0804.4139
 Günther, R., & Kley, W. 2002, *A&A*, 387, 550, arXiv:astro-ph/0204175
 Hachisu, I., Kato, M., & Nomoto, K. 1999, *ApJ*, 522, 487, arXiv:astro-ph/9902304
 Hinkle, K. H., Wilson, T. D., Scharlach, W. W. G., & Fekel, F. C. 1989, *AJ*, 98, 1820
 Ireland, M. J. et al. 2007, *ApJ*, 662, 651, arXiv:astro-ph/0703244
 Ivezić, Z., & Elitzur, M. 1997, *MNRAS*, 287, 799, arXiv:astro-ph/9612164
 Jahanara, B., Mitsumoto, M., Oka, K., Matsuda, T., Hachisu, I., & Boffin, H. M. J. 2005, *A&A*, 441, 589
 Karovska, M., Hack, W., Raymond, J., & Guinan, E. 1997, *ApJ*, 482, L175
 Karovska, M., Schlegel, E., Hack, W., Raymond, J. C., & Wood, B. E. 2005, *ApJ*, 623, L137, arXiv:astro-ph/0503050
 Kley, W. 1998, *A&A*, 338, L37, arXiv:astro-ph/9808351
 Livio, M., & Warner, B. 1984, *The Observatory*, 104, 152
 Löhner, R. 1987, *Comput. Methods Appl. Mech. Eng.*, 61, 323
 Lubow, S. H., & Shu, F. H. 1975, *ApJ*, 198, 383
 Makita, M., Miyawaki, K., & Matsuda, T. 2000, *MNRAS*, 316, 906, arXiv:astro-ph/9809003
 Marengo, M., Karovska, M., Fazio, G. G., Hora, J. L., Hoffmann, W. F., Dayal, A., & Deutsch, L. K. 2001, *ApJ*, 556, L47, arXiv:astro-ph/0106344
 Mastrodemos, N., & Morris, M. 1998, *ApJ*, 497, 303
 Matthews, L. D., & Karovska, M. 2006, *ApJ*, 637, L49, arXiv:astro-ph/0512205
 McIntosh, G. C., & Rustan, G. 2007, *AJ*, 134, 2113
 Mellema, G., & Frank, A. 1997, *MNRAS*, 292, 795, arXiv:astro-ph/9710255
 Peplinski, A., Artymowicz, P., & Mellema, G. 2008, *MNRAS*, 386, 164, arXiv:0709.3622
 Plewa, T., & Müller, E. 2001, *Comp. Phys. Comm.*, 138, 101
 Podsiadlowski, P., & Mohamed, S. 2007, *Baltic Astronomy*, 16, 26
 Reimers, D., & Cassatella, A. 1985, *ApJ*, 297, 275
 Ryde, N., Gustafsson, B., Eriksson, K., & Hinkle, K. H. 2000, *ApJ*, 545, 945, arXiv:astro-ph/0008235
 Sandin, C., & Höfner, S. 2004, *A&A*, 413, 789, arXiv:astro-ph/0309822
 Soker, N. 2004, *MNRAS*, 350, 1366, arXiv:astro-ph/0402364

- Soker, N., & Zoabi, E. 2002, MNRAS, 329, 204, arXiv:astro-ph/0106301
- Solf, J., & Ulrich, H. 1985, A&A, 148, 274
- Steehhs, D., Harlaftis, E. T., & Horne, K. 1997, MNRAS, 290, L28, arXiv:astro-ph/9708005
- Theuns, T., Boffin, H. M. J., & Jorissen, A. 1996, MNRAS, 280, 1264, arXiv:astro-ph/9602089
- Theuns, T., & David, M. 1992, ApJ, 384, 587
- Theuns, T., & Jorissen, A. 1993, MNRAS, 265, 946
- Walder, R., Folini, D., & Shore, S. N. 2008, A&A, 484, L9, arXiv:0804.2628
- Willson, L. A., Garnavich, P., & Mattei, J. A. 1981, Informational Bulletin on Variable Stars, 1961, 1
- Winters, J. M., Le Bertre, T., Jeong, K. S., Helling, C., & Sedlmayr, E. 2000, A&A, 361, 641
- Woodward, P., & Colella, P. 1984, J. Comput. Phys., 54, 115